



EPA Public Access

Author manuscript

Sci Total Environ. Author manuscript; available in PMC 2023 December 10.

About author manuscripts

Submit a manuscript

Published in final edited form as:

Sci Total Environ. 2023 December 10; 903: 166538. doi:10.1016/j.scitotenv.2023.166538.

Dermal and oral exposure risks to heavy metals from 3D printing metal-fill thermoplastics

Anna M. Wade^{a,b}, Derek M. Peloquin^{b,1}, Joanna M. Matheson^c, Todd P. Luxton^{b,*}

^aOak Ridge Institute for Science and Education, 1299 Bethel Valley Road, Oak Ridge, TN 37830, USA

^bU.S. Environmental Protection Agency, Office of Research and Development, Center for Environmental Solutions and Emergency Response, 5995 Center Hill Avenue, Cincinnati, OH 45224, USA

^cU.S. Consumer Product and Safety Commission, 5 Research Place, Rockville, MD 20850, USA

Abstract

Manufacturing advancements in polymer printing now allow for the addition of metal additives to thermoplastic feedstock up to 80–90 % by weight and subsequent printing on low-cost desktop 3D printers. Particles associated with metal additives are not chemically bound to the plastic polymer, meaning these particles can potentially migrate and become bioavailable. This study investigated the degree to which two human exposure pathways, oral (ingestion) and dermal (skin contact), are important exposure pathways for metals (copper, chromium, and tin) from metal-fill thermoplastics used in consumer fused filament fabrication (FFF). We found that dermal exposure to copper and bronze filaments presents the highest exposure risk due to chloride (Cl⁻) in synthetic sweat driving copper (Cu²⁺) release and dissolution. Chromium and tin were released as micron-sized particles < 24 μm in diameter with low bioaccessibility during simulated oral and dermal exposure scenarios, with potential to undergo dissolution in the gastrointestinal tract based on testing using synthetic stomach fluids. The rate of metal particle release increased by one to two orders of magnitude when thermoplastics were degraded under 1 year of simulated UV weathering. This calls into question the long-term suitability of biodegradable polymers such as PLA for use in metal-fill thermoplastics if they are designed not to be sintered. The greatest exposure risk appears to be from the raw filaments rather than the printed forms, with the former having higher metal release rates in water and synthetic body fluids for all but one filament type. For brittle feedstock that requires greater handling, as metal-fill thermoplastics can be, practices

*Corresponding author. luxton.todd@epa.gov (T.P. Luxton).

¹Present address: U.S. Food and Drug Administration, Office of Regulatory Affairs, Forensic Chemistry Center, 6751 Steger Drive, Cincinnati, OH 45237, USA.

CRedit authorship contribution statement

Anna Wade: Writing – Original draft preparation, Investigation, Formal analysis, Visualization, Methodology. **Derek Peloquin:** Investigation, Formal analysis, Methodology. **Joanna Matheson:** Writing – Review & editing, Funding acquisition. **Todd Luxton:** Writing – Review & editing, Conceptualization, Funding acquisition, Project administration, Supervision.

Declaration of competing interest

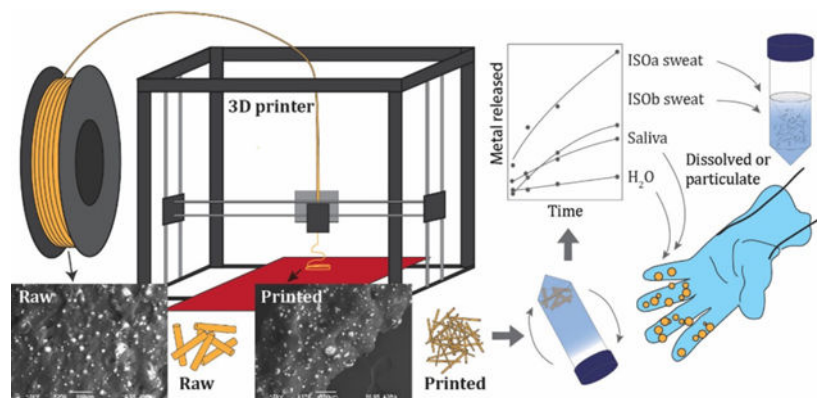
The authors declare that they have no known competing financial interests or personal relationships that could have appeared to influence the work reported in this paper.

Appendix A. Supplementary data

Supplementary data to this article can be found online at <https://doi.org/10.1016/j.scitotenv.2023.166538>.

common in metal powder 3D printing such as wearing gloves and washing hands may adequately reduce metal exposure risks.

GRAPHICAL ABSTRACT



Keywords

Additive manufacturing; Fused filament deposition; Human exposure; Metal additives; Metal bioaccessibility

1. Introduction

Fused filament fabrication (FFF), also known as fused deposition modeling, is a material extrusion process and the most popular type of additive manufacturing (AM)/3D printing. Low-cost 3D printers used in FFF can print with a variety of thermoplastic materials (most commonly polylactic acid, [-PLA], and acrylonitrile butadiene styrene, [-ABS]) with constraints only consisting of nozzle diameter and maximum printing temperature (typically <250 °C), making them ideal for small-scale production and home use (wikła et al., 2017; Tagliaferri et al., 2019). With the global AM market forecasted to expand at a compound growth rate of 20 % through 2030, and countries such as the U.S. listing AM as an emerging technology critical for national security, market demand for AM and for FFF will likely continue to grow (GVR, 2022; NTSC, 2022).

With this increased demand comes a need to assess the potential health effects from thermoplastic materials and printing processes. Literature on possible exposure risks from FFF has not kept up with the expanding market of novel materials and processes (Roth et al., 2019; Stefaniak et al., 2018). To date, research on adverse exposure effects from FFF printing have focused on the large number of ultrafine particles (UFPs are <100 nm) and hazardous volatile organic compounds (VOC) emitted during thermoplastic extrusion and printing processes (Azimi et al., 2016; Farcas et al., 2022; Farcas et al., 2020; Stephens et al., 2013). UFPs have been linked to acute respiratory infections, cardiovascular diseases, and lung cancer (Oberdörster et al., 2005). Adverse health effects from VOCs include a range of illnesses from mild irritation to respiratory diseases and cancer (Rumchev et al., 2007). Thermoplastics such as ABS and PLA are known to release polymer breakdown

products during extrusion that can become toxins upon release (Floyd et al., 2017; Kim et al., 2015). The number of emitted UFPs and VOCs, of particular concern for desktop 3-D printers with inadequate ventilation, has led researchers to conclude that inhalation is the main path of exposure for extrusion-based AM processes such as FFF (Bours et al., 2017; Floyd et al., 2017). However, few studies exist on health hazards outside of emissions from thermoplastic extrusion, leaving knowledge gaps for common exposure conditions (Roth et al., 2019).

Metal additives are one understudied component of the health risks associated with consumer FFF printing (Alberts et al., 2021). Thermoplastics, like all plastic products, contain chemical substances (known as “additives”) that improve polymer properties such as ductility and conductivity and are meant to prolong product life (Hahladakis et al., 2018). Metal additives, typically as fine atomized metal powders with average diameters on the order of microns to hundreds of nanometers, are mixed with polymer pellets, and the resulting metal/polymer mixture is melted into feedstock (Turner and Filella, 2021). These metal powder particles are not chemically bound to the plastic polymer and can potentially migrate to the environment (Hahladakis et al., 2018; Meng et al., 2021). Because the surface area of these micro-sized particles is important for dissolution, significant oxidative reactions may occur in a short time if these metal powders are exposed to aqueous solutions or body fluids, increasing bioavailability (Flint, 1998). Metal additives can be incorporated into thermoplastic feedstock either in trace concentrations (for color, UV-resistance, or other properties) or anywhere from 10 to 80 % by weight, known as “metal-fill” filaments (Tedla et al., 2022; Tedla and Rogers, 2023). Metal FFF printing has two post-printing steps – debinding and sintering – that dissolve and subsequently burn away the plastic polymer binding material and solidify the metal powder. However, because use of sintering ovens outside of manufacturing facilities is limited by high costs and low accessibility, manufacturers are now coming out with metal-fill thermoplastics designed to be polished.

Like ABS and PLA filaments, metal-fill thermoplastics present an inhalation exposure threat. Copper and bronze-fill thermoplastics emit particles and VOCs during the extrusion process at rates higher than their respective neat (i.e. only trace metal amounts) thermoplastics (Alberts et al., 2021; Floyd et al., 2017). These higher particle emissions are thought to stem from increased thermal conductivity in the copper feedstock that triggers higher temperatures and subsequently greater emission rates around the nozzle during extrusion (Tedla et al., 2022). Oral ingestion and dermal exposure are other important exposure pathways in AM (Roth et al., 2019) but have received less attention within the literature. The first known AM exposure assessment was a case of allergic contact dermatitis caused by cumulative exposure from the vat photopolymerization process, another AM method (Chang et al., 2004). More recently, another study confirmed workplace exposure to metal particles, ranging in size from 15 to 45 μm , when handling feedstock for powder bed fusion (Graff et al., 2017). For FFF specifically, dermal exposure is a likely exposure pathway for metal additives that are too large to be aerosolized. Alberts et al. (2021) failed to find copper or tungsten metal additives in SEM particle collection filters and suggested that copper and tungsten additives remained within the extruded feedstock. Vance et al. (2017) did not identify a discernible copper peak in the Raman spectra of aerosols emitted from copper-infused PLA (21 % copper by weight), concluding that copper additives affect

aerosol emissions but do not partition into the aerosol fraction. The lack of research on dermal exposure from FFF methods is perhaps attributable to the fact that only recently has the use of FFF with metal-fill filaments gained popularity (Tosto et al., 2021).

This study investigates the degree to which two main human exposure pathways, oral (ingestion) and dermal (skin contact), are important exposure pathways for metal-fill filaments. Raw and printed thermoplastic feedstock filaments infused with copper, bronze and stainless-steel fine metal powder were subjected to 2-hour release scenarios that included contact with water, synthetic sweat, and synthetic saliva, and a 1-hour exposure to synthetic stomach fluid. Concentration, particle size, and speciation of metal additives in these leachates were determined using total metals analysis, sequential filtration, electron microscopy, and X-Ray Absorption Near Edge Spectroscopy (XANES). We hypothesized that the metals contained within the metal infused filaments were susceptible to physical release and/or chemical oxidization and dissolution. Further, the release of metal particulates and oxidation byproducts may result in exposure of users to elevated concentrations of metals that may pose a human health risk. To test our hypothesis, we: (1) determined the bulk physicochemical properties of two different manufactured metal thermoplastic filaments; (2) compared leaching rates from different solutions including water and synthetic biological fluids before and post-production; and (3) estimated the bioaccessibility and bioavailability of non-aerosolized metal additives. Copper (Cu), chromium (Cr), and tin (Sn) were the metals used in this assessment due to their presence in the metal alloys. In this study, bioaccessibility (in vitro) refers to the fraction of a substance that is soluble in a synthetic biological media (e.g., artificial sweat, saliva, gastric fluid) and is available for absorption (Hedberg et al., 2010b). Bioavailability (in vivo) describes the fraction of the bioaccessible pool that is absorbed by humans, crossing the gastrointestinal epithelium (Ruby et al., 1999; US EPA, 2017). The bioaccessible fraction is a more conservative measure of toxicity, being larger than the bioavailable fraction due to incomplete absorption into the bloodstream (Ruby et al., 1996).

2. Materials and methods

2.1. Printer and feedstock

Six different metal/polymer filaments from two manufacturers were selected for analysis, labeled Manufacturer A (Man. A) and B (Man. B). Three of the metal filaments were composites of PLA/polyhydroxyalkanoate [PHA] from one manufacturer (Man. A) with copper (1.75 mm, 4.0 g/cm³, 90–97.5 % metal by weight according to manufacturer, personal communication), bronze (alloy of copper and tin, 1.75 mm, 3.9 g/cm³, 85–97.5 % metal by weight according to manufacturer, personal communication), and 410L stainless-steel additives (alloy comprising mostly of iron, chromium, manganese and silicon, 1.75 mm, 3.13 g/cm³, % by weight not available) with the % metal in the filament not specified. These filaments were designed to be sanded and polished after printing, with the base polymer matrix remaining. The other three metal/polymer filaments were pure PLA composites from a different manufacturer (Man. B) with copper (1.75 mm, 4.5 g/cm³, 87.0–90.7 % metal by weight according to manufacturer), bronze (1.75 mm, 4.5 g/cm³, 88.0–90.0 % metal by weight), and 316L stainless-steel additives (alloy comprising mostly

of iron, chromium, nickel, molybdenum, and manganese, 1.75 mm, 3.5 g/cm³, 80.0–85.0 % metal by weight). These filaments can be sintered post printing, removing up to 98 % of the thermoplastic binder, which comprises anywhere between 8 and 20 % of the feedstock by weight. The main differences in grade specifications for 316L and 410L stainless steel are a higher Cr content for 316L (16–18 % weight) than for 410L (11–13.5 % Cr), and a higher nickel (Ni) content for 316L (10–14 %) than 410L (max 0.60 %). Because of its higher Cr and Ni alloy content, Man. B stainless steel filament likely has greater corrosion and oxidation resistance than the Man. A stainless-steel filament. Full grade specifications are in supporting information (SI), in Table A.1. To distinguish between copper filament (raw and printed, solid) and the chemical element copper (released from filament), only the latter will be abbreviated as Cu. Filaments were extruded from a LulzBot TAZ 6 FFF printer (Aleph Objects Inc., Loveland, CA) using a 0.5 mm steel nozzle toolhead with a print speed between 35 and 45 mm/s. Extrusion temperatures were set at recommended temperatures by manufacturers: 200 °C for the metal PLA/PHA composites, and 210 °C for metal PLA composites and neat PLA.

2.2. Characterization methods

Total elemental abundance of metals present in the filaments was determined by microwave assisted acid digestion with three replicates. Digestions were performed using TFM iPrep digestion vessels (CEM Corporation) with 9 mL of HNO₃ and 3 mL of HCl that were heated to 200 ± 5 °C with a 20-minute ramp time and 20-minute hold time. iPrep vessels have a maximum pressure of 1500 psi (103 bar) versus 500 psi (35 bar) for the MARS Xpress vessels and withstood all digestions without any venting of contents. After digestion, all supernatants were collected and diluted to 50 mL with ultrapure water from a Super-Q water purification system (Millipore Sigma, Burlington, MA) and stored at 4 ± 2 °C in 50 mL polypropylene centrifuge tubes (Fisher Scientific).

Total metal concentrations of the acid digests, filtered, and unfiltered samples were measured using an Agilent 7900 ICP-MS (Agilent Technologies, Santa Clara, CA) with either no gas or helium collision mode depending on the element in accordance with EPA Method 6020B (US EPA, 2014). Analysis of matrix spikes (spike recovery 100 ± 20 %), analysis of certified second source standards (100 ± 20 % of certified value), and method blanks were used for quality assurance/quality control. Extractions were performed with three replicates and where coefficient of variation (CV) >100 % for metal concentrations of interest (Cr, Cu, and Sn) on the ICP-MS, repeated for a second analysis.

Metal particle size and shape from raw and printed thermoplastics were analyzed by field emission scanning electron microscopy (SEM) (JEOL JSM-7600F, Tokyo, Japan) in Secondary Electron Imaging (SEI) and Backscatter Electron Imaging (BEC). Metal particles were collected on aluminum SEM stubs with carbon low contaminant spectro-tabs attached (Agar Scientific, Stansted, U.K.). This was done by pressing raw filament to the stubs from both the curved filament surface as well as cross-sectional areas from freshly cut pieces. Two to three stubs were prepared for each filament type, and a total of 20 SEM images taken for each filament type. The SEM operated at 15 kV with a 2 nm resolution, and samples were imaged at 50×–5000× magnification. For particle size, SEM images

were processed using the software ImageJ, a public domain image processing and analysis program developed at the National Institute of Health (NIH) (Schindelin et al., 2012). This was done by converting grayscale images to a binary image with a lower threshold cutoff ≈ 100 and upper cutoff of ≈ 255 with the dark background option. Sizes of the particles were determined using ImageJ's particle analysis package with circularity from 0.3 to 1. Diameter was estimated based on calculated area for each particle, assuming a spherical approximation, and total number of particles measured for diameter was 2809. An example set of images is shown in the SI (SI Fig. A.1). To estimate specific surface area (SSA) values for the metal particles, excluding the thermoplastic matrix, the mass of an individual particle was calculated using alloy densities (copper $\sim 8.96 \text{ g/cm}^3$, bronze $\sim 8.73 \text{ g/cm}^3$, 316L steel $\sim 8 \text{ g/cm}^3$, and 410L steel $\sim 7.16 \text{ g/cm}^3$) and mean diameters from SEM analysis. Using this estimated mass of a particle, the number of particles per gram and combined surface area of these particles (assuming a sphere) was subsequently estimated (Table 2).

2.3. Simulated leaching and weathering experiments

2.3.1. Leaching experiments—Estimates of metal exposure were determined by leaching materials with DI water, artificial saliva (oral exposure), and two types of artificial sweat (dermal exposure). For each experiment, $2 \pm 0.005 \text{ g}$ of unprinted raw filament (hereby referred to as “filament”) or extruded/printed filament (referred to as “printed”) were cut into 1 cm long pieces and extracted in 40 mL of solution. The solid-to-liquid extraction ratio of 1:20, following the USEPA Toxicity Characteristic Leaching Procedure (TCLP), was used to ensure soluble metals remained well below saturation limits (US EPA, 1986). Samples were rotated at 30 rpm in 50 mL trace metal grade centrifuge tubes, and 1 mL samples taken at 15, 30, 60 and 120 min and preserved with 5 % HNO_3 (HNO_3 69 %, reagent grade, Sigma-Aldrich). Triplicates, matrix spikes, and method blanks were used to assess accuracy and precision. The 2-hour limit is the standard time limit for the European standard EN 71 that is used to measure the migration of hazardous elements in toys (Weidenhamer et al., 2011). Leaching rates were normalized to surface area on a mg cm^{-2} basis given that, from a chemical and material viewpoint, metal release is a surface reaction. Surface area was calculated by multiplying the length of 2 g of filament (error $\pm 10 \text{ mm}$ for printed, error $\pm 1 \text{ mm}$ for raw) by the diameter. Average diameter, which was measured using SEM ($n = 10$), was 1.75 mm for raw filament and 0.5 mm for printed filament. The surface area contribution from cross-sectional faces of cut pieces was minor relative to the contribution from filament length ($\sim 5 \%$) and was not included in the calculations.

Artificial saliva was prepared according to Standard EUR 19899 EN (2001) by the General Directorate Joint Research Center of the European Commission. Two artificial sweat solutions were prepared according to the formulation in “ISO 105-E04:2013 Textiles – Tests for Color Fastness – Part E04: Color Fastness to Perspiration” from the International Organization for Standardization (ISO) at $\text{pH } 5.5 \pm 0.2$ (Sweat ISOa) for the acidic formulation and $\text{pH } 8.0 \pm 0.2$ (Sweat ISOb) for the basic formulation (SI Table A.2). While developed to test textile colorfastness to perspiration, the ISO artificial sweat solutions have been used to study chemical migration from different natural and synthetic polymer consumer products (Ge et al., 2021; Peloquin et al., 2020). Another common artificial

sweat formulation, developed for compliance testing like the ISO solutions, is the European Standard EN 1811 for nickel release from Ni-containing products (Hedberg et al., 2010b). For this study, the ISO formulations were chosen as they cover an appropriate range of pH, and contain an amino acid, which is important for metal dissolution (Harvey et al., 2010). While sweat composition varies widely based on age, gender, and anatomical location, material properties and exposure time override differences in artificial sweat formulations when it comes to estimating the bioaccessible fraction of heavy metals (Midander et al., 2016).

Artificial solutions were stored in high-density polyethylene bottles at room temperature (19–22 °C) and prepared fresh daily. A subset of samples was passed through a 0.45 µm membrane filter and a subsequent 10 kDa centrifugal filter (Millipore Amicon Ultra-15) with a ≈3 nm cutoff to divide metals into dissolved forms (<1 kDa), colloids (1 kDa–0.45 µm) and particles (>0.45 µm). To precondition the 10 kDa filters and avoid potential absorption of dissolved metals, an initial filtrate was passed through and discarded, followed by a second filtrate from which samples were taken.

2.3.2. IVBA—An in-vitro bioaccessibility (IVBA) assay was used to mimic the solubility of Cu, Cr and Sn when exposed to a simple extraction medium (0.4 M glycine buffer at pH 1.5 ± 0.5) that mimics gastrointestinal tract (GIT) fluids (US EPA, 2017). Developed for use in the assessment of lead relative bioavailability (RBA), the IVBA assay has been used to estimate potential exposure through the GIT following incidental ingestion of metals including Cu (Santiago-Rodríguez et al., 2015) and Cr (Wang et al., 2020). The approach, which used a solid-to-liquid ratio of 1:100, was to extract 0.5 g of raw filament in 50 mL of the extraction solution, adjust the pH to 1.5 and rotate at 30 rpm for 1 h at a constant temperature of 37 °C. Extracts were then run through 0.45 µm and 10 kDa filters. Only raw filaments, not printed, were analyzed because metal particle solubility upon exposure to gastrointestinal conditions was expected to be similar between the two forms. Due to physiological conditions (large volume of gastric juice, small amount of solid introduced), the solid to liquid ratios used for IVBA gastric extractions are often smaller than ratios for synthetic sweat or saliva extractions (Bradham et al., 2018; Quadros et al., 2013). However, for IVBA extractions, solid to liquid ratios ranging from 1:100 to 1:5000 have been found to have little effect on bioaccessibility (Hamel et al., 1998).

2.3.3. Weathering experiment—Metal filaments and extruded material were irradiated using a UV lamp (BHK Mercury Grid lamp, BHK Engineering, Product No. 977208) for simulation of UV-C sunlight at 254 nm, verified with a 254 ± 8 nm solar meter. Samples were placed in 40 mm diameter glass petri dishes 120 mm beneath the grid lamp and irradiance averaged 1950 µW/cm². 2 ± 0.005 gram raw and printed filaments (n = 3) were irradiated for approximately 220 h, during which samples were rotated and gently mixed in the petri dishes. Based on data from the National Solar Radiation Database (NSRD), the yearly-average insolation in Cincinnati, OH from 1998 to 2016 was 1551 kW h m⁻² (Sengupta et al., 2018). 220 h insolation with irradiance 1950 µW/cm² corresponded to 9.2 days of exposure, calculated by the following: $1950 \mu\text{W}/\text{cm}^2 \times (1 \text{ mW}/1000 \mu\text{W}) \times (1 \text{ kW}/1,000,000 \text{ mW}) \times (1000 \text{ cm}^{-2}/\text{m}^{-2}) \times 3600 \text{ s} = 7.02 \text{ kW h m}^{-2}$; $1551 \text{ kW h m}^{-2}/7.02$

$\text{kW h m}^{-2} \approx 220 \text{ h}$ or 9.2 days. Leaching with DI water was started within 30 min after irradiation ended.

2.4. XANES analysis

Raw filaments were sanded with 80 grit sanding discs and then homogenized by hand with a mortar and pestle. This powder was combined with polyvinylpyrrolidone (PVP), pressed into 1.3 mm pellets using a manual pellet press, and sealed in Kapton[®] polyimide tape. The 10 kDa filters, which captured the suspended particles greater than ~10 nm in size, were cut and then layered and sealed between Kapton polyimide tape. For the aqueous samples, clean Kimwipes were cut and loaded dry into sample racks, saturated with solution, and sealed with Kapton polyimide tape. Pellets were measured for Cr, Cu, and Sn K-edge at the Materials Research Collaborative Access Team (MRCAT) 10-BM line at the Advanced Photon Source (APS) operated by the U.S. Department of Energy (DOE) at Argonne National Lab (Lemont, IL). Energy of the incident X-rays was scanned using a Si(111) monochromator consisting of a water-cooled first crystal and a 50-mm long second crystal. Incident beam energies were calibrated to the first derivative inflection points of the absorption edges (5989 eV for Cr, 8979 eV for Cu, and 29,200 eV for Sn) for the metal reference foil standards. XANES spectra, 3–5 scans per sample, were collected from –200 eV below the respective adsorption edge to 550 eV above the respective edge. Spectra were merged, calibrated, and normalized using the software, Athena (Ravel and Newville, 2005). Normalization was done by fitting a first order polynomial from –150 to 30 eV below the edge and either a second or third order polynomial to spectra from 75 to 150 to 225–300 eV above the edge. Linear least-squares combination fitting (LCF) of the XANES region was performed in Athena on select spectra along with a library of reference compounds. The energy range for the fit was –20 to 30 eV above the edge. Quality of the fits was indicated by chi-square and the R factor. The average sensitivity of XANES LCF is 5 %, meaning any species with a chemical composition <5 % is speculative (Kelly et al., 2008).

2.5. Statistical analysis

All calculations and statistical analyses were performed in R (Team, 2022). All data were tested for normality (Shapiro-Wilk test). Statistical differences between datasets were measured using one-way ANOVA with Tukey's HSD test a posteriori, or Student's *t*-test, with *p* values < 0.05 significant. An unpaired *t*-test was used to determine if the average value of an element or metal present in the filament were statistically different ($m_1 = m_2$; $\alpha = 0.05$). Zero-order rate constants were calculated using simple linear regression models with 'dplyr,' 'broom,' and 'tidyr' packages.

3. Results and discussion

3.1. Physicochemical characterization of metal-fill filaments

Nominal composition of the metal filaments (Table 1) was 68 to 87 % metal infill, including additives, and 13 to 32 % thermoplastic binder. In addition to the expected elements for bronze, copper and stainless steel, other trace metals were present including arsenic (As), lead (Pb), antimony (Sb), and zinc (Zn). Man. B 316L stainless-steel filament had significantly more Cr ($p = 0.007$), Mo ($p < 0.0001$), and Ni ($p < 0.0001$) than Man. A

410L filament, which was confirmed that the former was a Cr-Ni-Mo austenitic alloy. Man. B bronze, copper, and stainless-steel filaments, which were designed to be sintered, all contained more total metal than the respective Man. A filament types, designed to be polished, but the differences between manufacturers were not significant at $p = 0.05$.

The metal infill for the filaments was present as micro-sized metallic spheres dispersed as metallic powder through the polymer matrix. Particles were spherical in shape, with a minor fraction having irregularities such as elongated or joined particles and indentations or smaller particles known as “satellites” agglomerating on the surface of larger particles (Barreto et al., 2022). These non-spherical particles were attributed to oxidation during the atomization process, which is when molten metals are rapidly broken into smaller metal droplets by high- velocity gas, water or plasma jets and solidified into powder (Ansell et al., 2021). Both manufacturers used metal powders produced by gas atomization in their feedstock, the most common technique used for producing powders in AM, including powders used in powder bed fusion. This process produces metal powders at an optimal cost but inevitably yields a fraction of non-spherical particles with irregular morphologies in the final product (Kassym and Perveen, 2020).

Particle size analysis based on SEM image analysis showed mean diameter to range from 7.8 μm to 24.0 μm for the micron sized fraction, with distributions skewed to the smaller sizes (Table 2). Man. B filament had larger copper and stainless-steel particles (12.4 μm and 24.0 μm) than Man. A filament (9.4 μm and 7.8 μm). In contrast, bronze particles were larger in the Man. A filament (19.8 μm) than in the Man. B filament (12.3 μm). These differences are important for oxidation rates, as smaller particles are more impacted by surface oxidation and other surface chemical reactions than larger particles due to having a higher oxide fraction by mass. Chromium and manganese oxides have been found on the surface of gas atomized 316L stainless steel powders used in AM (Riabov et al., 2020). Oxide thickness on pure Cu powder used in laser powder bed fusion (99.7–99.95 % Cu wt%) starts out anywhere from 2 to 15 nm in thickness and increases following each printing cycle (Bojestig et al., 2020). Based on SEM images, this metal infill is non-uniformly distributed (SI Fig. A.2). This is a common problem for thermoplastic fillers such as metal powders, especially when there are varieties in particle size (Masood and Song, 2004; Valino et al., 2019). This poor filler distribution likely explains some of the high variability in leached metal concentrations from all filament types (Table 3).

As expected, Cr, Cu and Sn species in the raw filament were primarily metallic based on analysis of the XANES region (SI Fig. A.3). The Cu K- edge for copper and bronze filaments was nearly identical to the metallic copper foil reference, suggesting minimal oxidation had occurred during atomization and filament fabrication. The energy position of the Cr absorption K-edge for both 316L and 410L stainless steel types showed no shift in comparison to the metallic Cr foil. However, the subsequent XANES region (within 100 eV of the edge) was starkly different between the two alloys, likely due to different crystal structures. The martensitic 410L alloy (Man. A) has its chromium atoms in a body-centered cubic structure whereas the austenitic 316L alloy (Man. B) has chromium atoms in a face-centered cubic crystal structure due to the inclusion of Ni. Finally, the Sn K-edge for the Man. A and Man. B bronze filament resembled a mixture of tin(IV) oxide and metallic

Sn, the former likely from cassiterite (SnO_2), which is the principal source for Sn metal (79.6 % Sn) and commonly used in bronze metallurgy (Haldar, 2020). Both bronze filaments exhibited a clear increase in white line intensities, characteristic of oxide species, from the Sn foil reference but with reduced intensities compared to the SnO_2 standard as well as a slight energy shift toward lower energies, reflecting the inclusion of metallic Sn. XANES is a bulk measurement of the metal powder speciation, so the nanometer thick oxide layer that forms on the particle surface during the atomization process is not visible on micro-sized particles (Fleischmann et al., 2022; Hryha et al., 2018). Subsequent solid-state processing, such as sintering, is meant to reduce and decompose these metal oxides before the particles are fused together but the process is not 100 % efficient (Chasoglou et al., 2013).

3.2. Cu, Sn and Cr release from filaments in different solutions

Table 3 shows total Cu, Sn and Cr concentrations, including soluble and particulate fractions, released from printed or raw filament (normalized to 1 g) into different synthetic fluids following 2-hour exposure scenarios. Released Cu concentrations were highest in synthetic sweat (maximum 327 μg Cu released per g of filament) in comparison to H_2O and synthetic saliva (maximum 76 and 95 $\mu\text{g g}^{-1}$, respectively). Maximum amounts of Sn and Cr released were low (25.7 $\mu\text{g g}^{-1}$ and 6.99 $\mu\text{g g}^{-1}$) and showed less release in synthetic sweat. Figs. 1 and 2 demonstrate the increase in Cu and Cr concentrations for copper and stainless-steel filaments over this 2-hour period. Copper and Sn release from bronze filaments followed similar trends to the copper filament, the data for which is in the SI (Fig. A.4). Copper release patterns did not appear to differ based on manufacturer. Despite a lower Cr content, the 410L raw filament (Man A., ~8 % Cr by weight) released significantly more Cr than the 316L raw filament (Man. B, ~13 % Cr by weight).

During this 2-hour period, Man. A filament released higher concentrations of Cr, Cu, and Sn than printed Man. A material, despite the latter having a surface area 3 \times higher (Table 3). Furthermore, when normalized to surface area (the estimates for which are shown in Table 3), all but one of the filament types released more total metal in its raw form than in the printed form (SI Table A.4). The reason for these results could be due to differences in the number of metal particles that are loosely bound to the exterior of the thermoplastic, causing greater initial loss (2 h in this case) of metal particles from raw metal-fill feedstock. Previous research has hypothesized about a “leachable layer” of metal additives from polymer products that is a byproduct of contamination during the manufacturing process (Turner and Filella, 2021). Examples include the initial pulse of antimony (Sb), which is used as a catalyst in the production of polyethylene terephthalate (PET), released from new unwashed PET bottles (Cheng et al., 2010). In this case, the higher pulse of metal particles from raw thermoplastic feedstock may be a legacy effect from the production process, wherein a certain fraction of metal particles are poorly affixed to the polymer matrix.

Solution chemistries had a significant impact on Cu release. Synthetic sweat (ISOa and ISOb) increased the amount of total released Cu, particulate and dissolved, by an order of magnitude in comparison to H_2O and synthetic saliva. Differences in Cu were not immediately apparent after the initial 15 min, suggesting chemical dissolution rather than an immediate physical loss (Fig. 1). Artificial sweat contained chloride (~1850 mg L^{-1}), a

strong Cu corrosion catalyst, as well as *L*-histidine, an amino acid that chelates Cu, both of which would hasten Cu release (Boulay and Edwards, 2001; Deschamps et al., 2005). Chloride (Cl) is an aggressive anion that is known to break down the passivating oxide layer on metals and alloys (Hoar and Jacob, 1967). Cu release from copper filaments after 2 h and Cl concentration (0, 365 and 1850 mg L⁻¹ for H₂O, synthetic saliva, and synthetic sweat, respectively) had a significant positive relationship ($p < 0.05$, $r^2 > 0.95$, SI Fig. A.5). This suggests Cl is driving the Cu release from copper filaments, although the relationship was not significant for bronze filaments. Less chloride (~365 mg L⁻¹) may explain why artificial saliva did not have as marked of an impact on Cu release from copper and bronze filaments.

The response of Sn to different solutions was highly correlated to Cu loss. For bronze filaments, Sn release increased linearly with Cu release ($r^2 = 0.67$, $F_{1,176} = 366.5$, $p < 2e-16$). Proportionally less Sn was lost as compared to Cu based on the ratio of Sn:Cu in the raw filament, and this solution ratio decreased over the 2-hour period, likely due to incongruent dissolution (SI Fig. A.6). Sn is added to bronze alloy as a corrosion inhibitor (Chang et al., 2020; Liang et al., 2020). However, when normalized to the percentage of total Cu (Table 1), the percentage of Cu lost over the 2-hour period did not significantly differ between bronze and copper filaments, suggesting the addition of Sn does not impact Cu release.

Stainless-steel particles were more stable in the polymer matrix and were not as responsive to changes in solution type, as indicated by low amounts of Cr release across solutions (Fig. 2). Overall, 2-hr average concentrations across all solutions and filament types compromised 0.04 % (CV = 107 %) of the total bulk content (Tables 1 and 3). Previous research reported very small fractions of Cr released from particles of stainless steel in artificial sweat, attributing the lack to a chromium(III)-rich surface oxide creating an insoluble barrier (Hedberg et al., 2010b). In another study, localized corrosion of stainless steel occurred by chloride ions only at temperatures above 60 °C (Sim et al., 2017). Within the medical field, no effective chelating agent for metallic chromium has been identified (Smith, 2013). Different alloy grades may explain the greater total Cr release from Man. A steel filament, an austenitic steel with less corrosive resistance than the martensitic Man. B steel filament. Differences between the printed filaments may be due to particle size, as the larger Man. B steel particles may be more susceptible to physical release as the surface area of the matrix polymer increases upon printing.

3.3. Evidence for metal corrosion and speciation changes

Size fractionation data corroborated the notion of chemical dissolution for Cu while showing little evidence of any significant Cr and Sn dissolution in dermal and oral exposure scenarios. For Cu, the fraction of dissolved versus particulate Cu released into solution varied widely across solution types (SI Table A.5). Following 2-hour extractions, anywhere from 25 % to 100 % of the Cu released from copper and bronze filaments in H₂O was dissolved (passing through a 10 kDa membrane). This is likely due to the leaching of cupric ions (Cu²⁺), which will chelate with Cl⁻ forming stable solution complexes (Cuppert et al., 2006). Copper released in synthetic saliva was entirely particulate, with 10 kDa filtrates below the method detection limit (MDL) (~2 ppb), suggesting dissolution kinetics are either

longer than 2 h or potentially hindered by phosphate ($753 \text{ mg L}^{-1} \text{ K}_2\text{HPO}_4$) in the artificial saliva. Phosphates are frequently used for potable water treatment to reduce soluble copper and to inhibit corrosion (Edwards et al., 2002). In contrast, 100 % of the Cu released in synthetic sweat (ISOa) was dissolved. Size fractionation data for Cr and Sn showed little evidence of any substantial dissolution in H_2O , synthetic saliva, and synthetic sweat, with 10 kDa filtrates at or below MDLs for both metals. Thermodynamically, Sn(0) and Sn(IV) oxide ($\text{SnO}_2(\text{s})$) are very stable in near-neutral environments characteristic of artificial sweat and saliva (pH 5.5–8) (Séby et al., 2001). Metallic Cr and chromium(III) oxide are both highly insoluble, which explains why neither has been found to cause skin sensitization or irritation (Hedberg et al., 2010b).

Metallic particles underwent greater dissolution in the IVBA assay, suggesting potential for chemical changes upon ingestion and translocation to the gastrointestinal tract (pH 1.5). Sn underwent complete dissolution for both filament types (SI Table A.6). This is likely due to the dissolution of metallic Sn, known to dissolve to stable water-soluble Sn^{2+} in highly acidic solutions (Gerhátová et al., 2022). Cr also underwent complete dissolution from the martensitic steel (410L, Man. A) filament in the IVBA assay, as well as from the austenitic steel (316L, Man. B) albeit at far lower rates due to higher corrosion resistance (see release rates in Section 3.4). These results show that highly acidic, aggressive environments such as the gastric tract can potentially negate any corrosion resistance of these metal particles, even if solubility is minimal during oral and dermal exposure (Santiago-Rodríguez et al., 2015).

In terms of speciation, metallic Cu released from copper and bronze filaments in biological fluids and trapped on filters showed significant oxidation (Fig. 3). In synthetic sweat, metallic Cu released from copper and bronze filaments oxidized to species that closely resemble Cu(II)-organo acid complexes, Cu(II) hydroxide and Cu(II) oxide. Linear combination fitting (LCF) of the normalized XANES showed that 96 % of the Cu present was present as Cu(II) hydroxide, CuO, and Cu-Organic complexes such as Cu-histidine with trace amounts (<5 %) of raw filament present (SI Table A.7). Of the Cu(II) reference spectra considered, Cu-hydroxide, Cu-histidine and CuO were the predominant Cu species found after exposure to synthetic sweat. Copper oxidation proceeded rapidly – a sample of Man. A copper filament exposed to synthetic sweat for 1 h showed complete oxidation of metallic Cu to Cu(II) species similar to $\text{Cu}(\text{OH})_2$, Cu(II)-organic complexes and CuO (SI Fig. A.7). Copper oxidation occurred in a modified IVBA assay, carried out at room temperature, with about 50 % of the Cu oxidizing to Cu(I) or Cu(II) species after 1 h. Copper bound to lactic acid, Cu(I) oxide and Cu(II) oxide were the most common species identified. Lactic acid is a known degradation product of PLA upon hydrolysis and contact with biological media (Da Silva et al., 2018).

Speciation of Cr and Sn did not show any marked changes in oxidation state after exposure to synthetic sweat or saliva, although the spectra were of poor quality due to low element concentration. For Sn, this is likely due to the stability of Sn(IV) oxide over a wide pH and conductivity range (Hutchison and Scully, 2018). For Cr, it is likely due to the passivating layer of chromium oxide, Cr_2O_3 . In the IVBA assay, dissolved Cr (<10 kDa) was too low to be analyzed for XANES in solution. This dissolved fraction was likely chromium

oxide, based on previous studies that found Cr released as Cr(III) from 316L-stainless steel (Hedberg et al., 2010).

3.4. Connecting release rates to potential exposure scenarios

The physicochemical form of released metals plays a critical role in exposure potential. Generally, dissolved metal species will be more bioaccessible than particulate forms since the former is more readily absorbed (Reeder et al., 2006). However, the micron-scale diameter of these metal particles gives them high potential for dermal adherence. As demonstrated with soils, most particles that adhere to the hand are $<50\ \mu\text{m}$ in size (Madrid et al., 2008; Sheppard and Evenden, 1994; Yamamoto et al., 2006). This incidental exposure by way of dermal adherence and subsequent hand-to-mouth activity can lead to soil ingestion rates of 1 to $>100\ \text{mg/day}$ (Deubner et al., 2001).

To evaluate exposure risks, a simple rate was calculated by fitting a linear regression between metal release and exposure time, with rates in $\text{mg cm}^{-2}\ \text{min}^{-1}$. Model fits were significant ($p < 0.05$) for Cu release from copper and bronze filaments in H_2O and synthetic sweat but not in synthetic saliva (SI Table A.8). Model fits were poorer for Sn and Cr release from bronze and stainless-steel filaments. Those rates with significant to marginally significant fits ($p \leq 0.10$) were subsequently converted to mg h^{-1} and scaled up to a 5 cm cube with a $150\ \text{cm}^2$ surface area to mimic a 3-D printed object. This conversion was done for both raw and printed filaments to compare estimated release rates on a larger hypothetical scale.

Raw copper filaments had significantly higher release rates of Cu than printed filaments, particularly in synthetic sweat (Fig. 4). Upon exposure to H_2O , a 5 cm cube of raw Man. A copper filament is estimated to release 1 mg of Cu in 1 h, in comparison to 0.05 mg from a printed Man. A copper filament. Upon exposure to synthetic sweat (ISOa), these rates increase to $3.30\ \text{mg h}^{-1}$ from raw filament and $0.26\ \text{mg Cu h}^{-1}$ from printed; among the printed types, the highest estimated release rate of Cu was from Man. B bronze, with $1.41\ \text{mg Cu h}^{-1}$ from a 5-cm cube. Among the stainless-steel filaments, Man. A steel filament had the highest release rate of Cr in synthetic sweat, with $0.06\ \text{mg Cr h}^{-1}$ from a 5-cm cube (See Table A.8).

Among the three metals analyzed, Cu had the highest migration rates due to its high concentrations and tendency to solubilize. While an essential nutrient at low concentrations, acute ingestion of excess Cu causes deleterious health effects (Taylor et al., 2020). Gastrointestinal symptoms such as nausea or abdominal pain occur in humans from concentrations as low as $4\text{--}6\ \text{mg Cu L}^{-1}$ within 15 min of exposure (Araya et al., 2001; Olivares et al., 2001). Because of these health effects, the U.S. National Academy of Medicine set Tolerable Upper Intake Levels (TUILs) for Cu ranging from $1000\ \mu\text{g/day}$ for children 1–3 years old to $10,000\ \mu\text{g/day}$ for adults 19 years (Trumbo et al., 2001). TUIL values indicate the highest level of Cu intake that is likely to pose no risk of adverse health. In this study, based on Tables 3, 1 g of Man. B Bronze filament ($\sim 10\ \text{cm}$ in length) could potentially release $>1000\ \mu\text{g}$ Cu in the GI tract. While this is a conservative estimate, it highlights the potential for acute short term Cu exposure from copper and bronze filaments.

For brittle feedstock, as metal-fill thermoplastics are prone to be (Woods, 2022), greater handling of the material is required during the printing process leading to possible higher dermal exposure than with neat thermoplastics (low metal). Given the high solubility of the Cu, extended exposure should be limited to prevent any gastrointestinal effects during the handling and printing process. NIOSH, in a publication for 3D printing with metal powders, such as metal powder fusion, recommended nitrile gloves and other personal protective equipment for workplaces (Glassford et al., 2020). For FDM of metal-fill thermoplastics, practices such as wearing gloves and washing hands may adequately reduce exposure during the printing and post-printing steps.

3.5. Impact of weathering on metal release

Release of metal additives is predicted to increase upon plastic UV aging due to increases in porosity and surface area of the matrix (Turner and Filella, 2021; Zhang et al., 2018). Prolonged exposure to UV light causes oxidative chain scission (degradation of the main polymer chain), increasing the brittleness and the hydrolysis of PLA (Agustin-Salazar et al., 2014; Copinet et al., 2004). In this study, simulated weathering of the thermoplastic for approximately one year disrupted the polymer's surface structure, accelerating the loss of metal particles by increasing porosity and surface area of the matrix. The coarse brittle surface of the aged, UV-weathered plastics is clear, exposing metal particles (Fig. D in SI Fig. 2.A).

This UV degradation process increased leachable concentrations of Cr, Cu and Sn metal additives from both raw and printed filaments by one to two orders of magnitude (SI, Table A.9). When exposed to H₂O, Cu concentrations leached from weathered copper filament over 2 h were approximately 2096 ppm (CV = 43 %) for Man. A filament and 3850 (CV = 40 %) for Man. B filament, about two orders of magnitude greater than unweathered filament (75 ppm (61 %) and 35 ppm (63 %), respectively). For stainless steel filaments, UV degradation had a greater impact on Man. A filament, both raw and printed, than on Man. B filament. Two-hour Cr concentrations in H₂O from Man. A filament were two orders of magnitude higher than the Man. B filament, reaching 46.8 ppm Cr (CV = 48 %) as opposed to 0.81 ppm (CV = 9 %) for raw filament. This greater susceptibility of the former may be attributed to structural differences between a PLA thermoplastic (Man. B filament) and a PLA/PHA thermoplastic (Man. A filament) that impact how polymer chains degrade, or due to differences in metal particle size. Filtration data showed metal loss to be entirely in particulate form. Less than 5 % of total Cu from weathered filaments passed through a 10 kDa filter, while Sn and Cr were at or below detection levels (SI Table A.9). This shows metal-fill thermoplastics have high potential for photooxidative degradation that increases the surface release of metal additives embedded in the matrix. Continued UV exposure of metal-fill 3D printed thermoplastics, coupled with moisture and heat fluctuations, may have significant deleterious effects upon thermoplastic physical properties. This calls into question the long-term tenability of using FFF to print metal-fill thermoplastic objects, especially ones using biodegradable polymers such as PLA, that are designed to be polished rather than sintered.

4. Conclusion

Metal additives are an understudied component of the health risks associated with consumer FFF, the most popular type of additive manufacturing. Here, we showed that metal-fill thermoplastics contain metal particles < 25 μm in diameter that have the potential to migrate and become bioavailable via dermal and oral exposure routes within 1 to 2 h. The highest exposure risk was dermal exposure to Cu^{2+} from copper and bronze filaments, believed to be caused by leaching induced by Cl^- in artificial sweat, a strong corrosion catalyst and chelating agent. Cr and Sn were more stable than Cu in the polymer matrix and were released as micron-sized particles with low bioaccessibility during oral and dermal exposure. Metal-fill thermoplastics showed significant degradation upon 1 year of simulated UV weathering, which increased the release of metal additives from both raw and printed material by one to two orders of magnitude. Prolonged UV exposure alongside moisture and heat fluctuations in household environments may degrade the mechanical properties and microstructure of metal-fill 3D printed thermoplastics in such a way that challenges the suitability of these materials for long-term use. Overall, the greatest exposure risk appears to be dermal exposure from raw filaments. Practices such as wearing gloves and frequent washing of hands, as well as safety measures used in metal powder bed fusion, may mitigate metal exposure risks during pre- printing steps.

Supplementary Material

Refer to Web version on PubMed Central for supplementary material.

Acknowledgements

This work was part of an interagency agreement between the U.S. EPA and the U.S. CPSC. This work has been subjected to EPA administrative review and approved for publication. The findings and conclusions in this paper are those of the authors and do not necessarily represent the views of the CPSC or EPA. Mention of trade names or commercial products does not constitute endorsement or recommendation for use. Thank you to the Advanced Photon Source (APS, Argonne, Illinois, USA) for the allocation of beam time. MRCAT operations are supported by the Department of Energy (DOE) and the MRCAT member institutions. Additionally, this project was supported in part by the Research Participation Program at the Office of Research and Development, U.S. Environmental Protection Agency, administered by the Oak Ridge Institute for Science and Education through an interagency agreement between the U.S. Department of Energy and U.S. EPA. We would like to thank Mahendra Arambewela, Logan Rand, Matt Noerpel, Aaron Betts, and Geoffrey Millard for technical support and assistance as well as Tyler Sowers and Phillip Potter for serving as internal reviewers.

Data availability

Data will be made available on request.

Abbreviations:

ABS	acrylonitrile butadiene styrene
AM	additive manufacturing
FFF	fused filament fabrication
GIT	gastrointestinal tract

IVBA	in-vitro bioaccessibility
PHA	polyhydroxyalkanoate
PLA	polylactic acid
RBA	relative bioavailability
SSA	specific surface area
TCLP	toxicity characteristic leaching procedure
UFP	ultrafine particles
VOC	volatile organic compounds
XANES	X-Ray Absorption Near Edge Spectroscopy

References

- Agustin-Salazar S, Gamez-Meza N, Medina-Juárez LÁ, Soto-Valdez H, Cerruti P, 2014. From nutraceuticals to materials: effect of resveratrol on the stability of polylactide. *ACS Sustain. Chem. Eng.* 2 (6), 1534–1542.
- Alberts E, Ballentine M, Barnes E, Kennedy A, 2021. Impact of metal additives on particle emission profiles from a fused filament fabrication 3D printer. *Atmos. Environ.* 244, 117956.
- Ansell TY, Hanneman T, Gonzalez-Perez A, Park C, Nieto A, 2021. Effect of high energy ball milling on spherical metallic powder particulates for additive manufacturing. *Part. Sci. Technol.* 39 (8), 981–989. 10.1080/02726351.2021.1876192.
- Araya M, McGoldrick MC, Klevay LM, Strain J, Robson P, Nielsen F, Poirier KA, 2001. Determination of an acute no-observed-adverse-effect level (NOAEL) for copper in water. *Regul. Toxicol. Pharmacol.* 34 (2), 137–145. [PubMed: 11603956]
- Azimi P, Zhao D, Pouzet C, Crain NE, Stephens B, 2016. Emissions of ultrafine particles and volatile organic compounds from commercially available desktop three-dimensional printers with multiple filaments. *Environ. Sci. Technol.* 50 (3), 1260–1268. 10.1021/acs.est.5b04983. [PubMed: 26741485]
- Barreto ES, Frey M, Wegner J, Jose A, Neuber N, Busch R, Uhlenwinkel V, 2022. Properties of gas-atomized Cu-Ti-based metallic glass powders for additive manufacturing. *Mater. Des.* 215, 110519.
- Bojestig E, Cao Y, Nyborg L, 2020. Surface chemical analysis of copper powder used in additive manufacturing. *Surf. Interface Anal.* 52 (12), 1104–1110.
- Boulay N, Edwards M, 2001. Role of temperature, chlorine, and organic matter in copper corrosion by-product release in soft water. *Water Res.* 35 (3), 683–690. [PubMed: 11228965]
- Bours J, Adzima B, Gladwin S, Cabral J, Mau S, 2017. Addressing hazardous implications of additive manufacturing: complementing life cycle assessment with a framework for evaluating direct human health and environmental impacts. *J. Ind. Ecol.* 21 (S1), S25–S36.
- Bradham KD, Diamond GL, Burgess M, Juhasz A, Klotzbach JM, Maddaloni M, Stifelman M, 2018. Soil arsenic in vivo and in vitro oral bioavailability methods for use in human health risk assessment, a review of the state of the science. *J. Toxicol. Environ. Health Part B Crit. Rev.* 21 (2), 83.
- Chang T-Y, Lee LJ-H, Wang J-D, Shie R-H, Chan C-C, 2004. Occupational risk assessment on allergic contact dermatitis in a resin model making process. *J. Occup. Health* 46 (2), 148–152. 10.1539/joh.46.148. [PubMed: 15090690]
- Chang T, Maltseva A, Volovitch P, Wallinder IO, Leygraf C, 2020. A mechanistic study of stratified patina evolution on Sn-bronze in chloride-rich atmospheres. *Corros. Sci.* 166, 108477.

- Chasoglou D, Hryha E, Nyborg L, 2013. Effect of process parameters on surface oxides on chromium-alloyed steel powder during sintering. *Mater. Chem. Phys.* 138 (1), 405–415.
- Cheng X, Shi H, Adams CD, Ma Y, 2010. Assessment of metal contaminations leaching out from recycling plastic bottles upon treatments. *Environ. Sci. Pollut. Res.* 17, 1323–1330.
- Copinet A, Bertrand C, Govindin S, Coma V, Couturier Y, 2004. Effects of ultraviolet light (315 nm), temperature and relative humidity on the degradation of polylactic acid plastic films. *Chemosphere* 55 (5), 763–773. [PubMed: 15013682]
- Cuppett JD, Duncan SE, Dietrich AM, 2006. Evaluation of copper speciation and water quality factors that affect aqueous copper tasting response. *Chem. Senses* 31 (7), 689–697. [PubMed: 16840540]
- wikła G, Grabowik C, Kalinowski K, Paprocka I, Ociepka P, 2017. The Influence of Printing Parameters on Selected Mechanical Properties of FDM/FFF 3D-printed Parts. Paper Presented at the IOP Conference Series: Materials Science and Engineering.
- Da Silva D, Kaduri M, Poley M, Adir O, Krinsky N, Shainsky-Roitman J, Schroeder A, 2018. Biocompatibility, biodegradation and excretion of polylactic acid (PLA) in medical implants and theranostic systems. *Chem. Eng. J.* 340, 9–14. [PubMed: 31384170]
- Deschamps P, Kulkarni P, Gautam-Basak M, Sarkar B, 2005. The saga of copper (II)–L-histidine. *Coord. Chem. Rev.* 249 (9–10), 895–909.
- Deubner DC, Lowney YW, Paustenbach DJ, Warmerdam J, 2001. Contribution of incidental exposure pathways to total beryllium exposures. *Appl. Occup. Environ. Hyg.* 16 (5), 568–578. [PubMed: 11370936]
- Edwards M, Hidmi L, Gladwell D, 2002. Phosphate inhibition of soluble copper corrosion by-product release. *Corros. Sci.* 44 (5), 1057–1071.
- Farcas MT, McKinney W, Qi C, Mandler KW, Battelli L, Friend SA, Winn A, 2020. Pulmonary and systemic toxicity in rats following inhalation exposure of 3-D printer emissions from acrylonitrile butadiene styrene (ABS) filament. *Inhal. Toxicol.* 32 (11–12), 403–418. [PubMed: 33076715]
- Farcas MT, McKinney W, Coyle J, Orandle M, Mandler WK, Stefaniak AB, Hammer MA, 2022. Evaluation of pulmonary effects of 3-D printer emissions from acrylonitrile butadiene styrene using an air-liquid interface model of primary normal human-derived bronchial epithelial cells. *Int. J. Toxicol.* 41 (4), 312–328. [PubMed: 35586871]
- Fleischmann B, Chateau-Cornu J-P, Dembinski L, Gyss O, Bigot R, Danlos Y, Ghanbaja J, 2022. Influence of particle size on surface oxide of 316L stainless steel powders for hot isostatic pressing. *Materialia* 22, 101405. 10.1016/j.mtla.2022.101405.
- Flint GN, 1998. A metallurgical approach to metal contact dermatitis. *Contact Dermatitis* 39 (5), 213–221. [PubMed: 9840256]
- Floyd EL, Wang J, Regens JL, 2017. Fume emissions from a low-cost 3-D printer with various filaments. *J. Occup. Environ. Hyg.* 14 (7), 523–533. 10.1080/15459624.2017.1302587. [PubMed: 28406364]
- Ge J-L, Wang J-X, Wu C-C, Bao L-J, Zeng EY, 2021. Development of an in vitro model to simulate migration of organic contaminants from pad products to human sweat and enhance dermal exposure risk assessment. *Sci. Total Environ.* 795, 148827.
- Gerhátová Ž, Babincová P, Drienovský M, Pašák M, erni ková I, uriška L, Palcut M, 2022. Microstructure and corrosion behavior of Sn–Zn alloys. *Materials* 15 (20), 7210. [PubMed: 36295278]
- Glassford E, Dunn K, Dunn K, Hammond D, Tyrawski J, 2020. 3D Printing With Metal Powders: Health and Safety Questions to Ask (Publication No. 2020–114). U.S. Department of Health and Human Services, National Institute for Occupational Safety and Health, Cincinnati, OH.
- Graff P, Ståhlbom B, Nordenberg E, Graichen A, Johansson P, Karlsson H, 2017. Evaluating measuring techniques for occupational exposure during additive manufacturing of metals: a pilot study. *J. Ind. Ecol.* 21 (S1), S120–S129.
- GVR, G. V. R, 2022. Additive manufacturing market size, share & trends analysis report by component, by printer type, by technology, by software, by application, by vertical, by material, by region, and segment forecasts, 2022–2030. Retrieved from San Francisco, CA, USA: <https://www.grandviewresearch.com/industry-analysis/additive-manufacturing-market>.

- Hahladakis JN, Velis CA, Weber R, Iacovidou E, Purnell P, 2018. An overview of chemical additives present in plastics: migration, release, fate and environmental impact during their use, disposal and recycling. *J. Hazard. Mater.* 344, 179–199. [PubMed: 29035713]
- Haldar SK, 2020. *Introduction to Mineralogy and Petrology*. Elsevier, Amsterdam, the Netherlands.
- Hamel SC, Buckley B, Liou PJ, 1998. Bioaccessibility of metals in soils for different liquid to solid ratios in synthetic gastric fluid. *Environ. Sci. Technol.* 32 (3), 358–362.
- Harvey CJ, LeBouf RF, Stefaniak AB, 2010. Formulation and stability of a novel artificial human sweat under conditions of storage and use. *Toxicol. in Vitro* 24 (6), 1790–1796. [PubMed: 20599493]
- Hedberg Y, Gustafsson J, Karlsson HL, Möller L, Wallinder IO, 2010. Bioaccessibility, bioavailability and toxicity of commercially relevant iron-and chromium-based particles: in vitro studies with an inhalation perspective. *Part. Fibre Toxicol.* 7, 1–14. [PubMed: 20180970]
- Hedberg Y, Midander K, Odnevall Wallinder I, 2010b. Particles, sweat, and tears: a comparative study on bioaccessibility of ferrochromium alloy and stainless steel particles, the pure metals and their metal oxides, in simulated skin and eye contact. *Integr. Environ. Assess. Manag.* 6 (3), 456–468. [PubMed: 20821707]
- Hoar T, Jacob W, 1967. Breakdown of passivity of stainless steel by halide ions. *Nature* 216 (5122), 1299–1301.
- Hryha E, Shvab R, Gruber H, Leicht A, Nyborg L, 2018. Surface oxide state on metal powder and its changes during additive manufacturing: an overview. *Metallurgia Ital.* 3, 34–39.
- Hutchison M, Scully J, 2018. Patina enrichment with SnO₂ and its effect on soluble Cu cation release and passivity of high-purity Cu-Sn bronze in artificial perspiration. *Electrochim. Acta* 283, 806–817.
- Kassym K, Perveen A, 2020. Atomization processes of metal powders for 3D printing. *Mater. Today Proc.* 26, 1727–1733. 10.1016/j.matpr.2020.02.364.
- Kelly SD, Hesterberg D, Ravel B, 2008. Analysis of soils and minerals using X-ray absorption spectroscopy. In: *Methods of Soil Analysis. Part 5. Mineralogical Methods*, vol. 5. Soil Science Society of America, Madison, WI 53711, USA, pp. 387–463.
- Kim Y, Yoon C, Ham S, Park J, Kim S, Kwon O, Tsai P-J, 2015. Emissions of nanoparticles and gaseous material from 3D printer operation. *Environ. Sci. Technol.* 49 (20), 12044–12053. 10.1021/acs.est.5b02805.
- Liang Z, Jiang K, Zhang T, Dou Z, 2020. Corrosion behavior of Cu–Sn bronze alloys in simulated archeological soil media. *Mater. Corros.* 71 (4), 617–627.
- Madrid F, Biasioli M, Ajmone-Marsan F, 2008. Availability and bioaccessibility of metals in fine particles of some urban soils. *Arch. Environ. Contam. Toxicol.* 55, 21–32. [PubMed: 18058158]
- Masood SH, Song WQ, 2004. Development of new metal/polymer materials for rapid tooling using fused deposition modelling. *Mater. Des.* 25 (7), 587–594. 10.1016/j.matdes.2004.02.009.
- Meng J, Xu B, Liu F, Li W, Sy N, Zhou X, Yan B, 2021. Effects of chemical and natural ageing on the release of potentially toxic metal additives in commercial PVC microplastics. *Chemosphere* 283, 131274.
- Midander K, Julander A, Kettelarij J, Lidén C, 2016. Testing in artificial sweat—is less more? Comparison of metal release in two different artificial sweat solutions. *Regul. Toxicol. Pharmacol.* 81, 381–386. [PubMed: 27664322]
- NTSC, N. S. a. T. C., 2022. Critical and emerging technologies list update. Retrieved from Washington, DC: <https://www.whitehouse.gov/ostp/news-updates/2022/02/28/nstc-critical-emerging-technologies-list-update/>.
- Oberdörster G, Oberdörster E, Oberdörster J, 2005. Nanotoxicology: an emerging discipline evolving from studies of ultrafine particles. *Environ. Health Perspect.* 113 (7), 823–839. [PubMed: 16002369]
- Olivares M, Araya M, Pizarro F, Uauy R, 2001. Nausea threshold in apparently healthy individuals who drink fluids containing graded concentrations of copper. *Regul. Toxicol. Pharmacol.* 33 (3), 271–275. [PubMed: 11407930]
- Peloquin DM, Baumann EJ Jr., Luxton TP, 2020. Multi-method assessment of PVP-coated silver nanoparticles and artificial sweat mixtures. *Chemosphere* 249, 126173.

- Quadros ME, Pierson IV R, Tulve NS, Willis R, Rogers K, Thomas TA, Marr LC, 2013. Release of silver from nanotechnology-based consumer products for children. *Environ. Sci. Technol.* 47 (15), 8894–8901. [PubMed: 23822900]
- Ravel B, Newville MA, 2005. ATHENA, ARTEMIS, HEPHAESTUS: data analysis for X-ray absorption spectroscopy using IFEFFIT. *J. Synchrotron Radiat.* 12 (4), 537–541. [PubMed: 15968136]
- Reeder RJ, Schoonen MA, Lanzirrotti A, 2006. Metal speciation and its role in bioaccessibility and bioavailability. *Rev. Mineral. Geochem.* 64 (1), 59–113.
- Riabov D, Hryha E, Rashidi M, Bengtsson S, Nyborg L, 2020. Effect of atomization on surface oxide composition in 316L stainless steel powders for additive manufacturing. *Surf. Interface Anal.* 52 (11), 694–706.
- Roth GA, Geraci CL, Stefaniak A, Murashov V, Howard J, 2019. Potential occupational hazards of additive manufacturing. *J. Occup. Environ. Hyg.* 16 (5), 321–328. 10.1080/15459624.2019.1591627. [PubMed: 30908118]
- Ruby MV, Davis A, Schoof R, Eberle S, Sellstone CM, 1996. Estimation of lead and arsenic bioavailability using a physiologically based extraction test. *Environ. Sci. Technol.* 30 (2), 422–430.
- Ruby MV, Schoof R, Brattin W, Goldade M, Post G, Harnois M, Carpenter M, 1999. Advances in evaluating the oral bioavailability of inorganics in soil for use in human health risk assessment. *Environ. Sci. Technol.* 33 (21), 3697–3705.
- Rumchev K, Brown H, Spickett J, 2007. Volatile organic compounds: do they present a risk to our health? *Rev. Environ. Health* 22 (1), 39–56. [PubMed: 17508697]
- Santiago-Rodríguez L, Griggs JL, Bradham KD, Nelson C, Luxton T, Platten WE, Rogers KR, 2015. Assessment of the bioaccessibility of micronized copper wood in synthetic stomach fluid. *Environ. Nanotechnol. Monit. Manag.* 4, 85–92. 10.1016/j.enmm.2015.07.003.
- Schindelin J, Arganda-Carreras I, Frise E, Kaynig V, Longair M, Pietzsch T, Cardona A, 2012. Fiji: an open-source platform for biological-image analysis. *Nat. Methods* 9 (7), 676–682. 10.1038/nmeth.2019. [PubMed: 22743772]
- Séby F, Potin-Gautier M, Giffaut E, Donard OFX, 2001. A critical review of thermodynamic data for inorganic tin species. *Geochim. Cosmochim. Acta* 65 (18), 3041–3053.
- Sengupta M, Xie Y, Lopez A, Habte A, Maclaurin G, Shelby J, 2018. The national solar radiation data base (NSRDB). *Renew. Sust. Energ. Rev.* 89, 51–60.
- Sheppard S, Evenden W, 1994. Contaminant enrichment and properties of soil adhering to skin. *J. Environ. Qual.* 23, 604–613.
- Sim J-H, Kim Y-S, Cho I-J, 2017. Corrosion behavior induced by LiCl-KCl in type 304 and 316 stainless steel and copper at low temperature. *Nucl. Eng. Technol.* 49 (4), 769–775.
- Smith SW, 2013. The role of chelation in the treatment of other metal poisonings. *J. Med. Toxicol.* 9, 355–369. [PubMed: 24113858]
- Stefaniak A, Johnson AR, Du Preez S, Hammond DR, Wells J, Ham JE, Plessis JL, 2018. Evaluation of emissions and exposures at workplaces using desktop 3-dimensional printer. *J. Chem. Health Saf.* 26 10.1016/j.jchas.2018.11.001.
- Stephens B, Azimi P, El Orch Z, Ramos T, 2013. Ultrafine particle emissions from desktop 3D printers. *Atmos. Environ.* 79, 334–339.
- Tagliaferri V, Trovalusci F, Guarino S, Venettacci S, 2019. Environmental and economic analysis of FDM, SLS and MJF additive manufacturing technologies. *Materials* 12 (24), 4161. [PubMed: 31835783]
- Taylor AA, Tsuji JS, Garry MR, McArdle ME, Goodfellow WL, Adams WJ, Menzie CA, 2020. Critical review of exposure and effects: implications for setting regulatory health criteria for ingested copper. *Environ. Manag.* 65 (1), 131–159.
- Team R, 2022. RStudio: Integrated Development Environment for R. RStudio, PBC, Boston, MA. Retrieved from. <http://www.rstudio.com/>.
- Tedla G, Rogers K, 2023. Characterization of 3D printing filaments containing metal additives and their particulate emissions. *Sci. Total Environ.* 875, 162648.

- Tedla G, Jarabek AM, Byrley P, Boyes W, Rogers K, 2022. Human exposure to metals in consumer-focused fused filament fabrication (FFF)/3D printing processes. *Sci. Total Environ.* 814, 152622 10.1016/j.scitotenv.2021.152622.
- Tosto C, Tirillò J, Sarasini F, Cicala G, 2021. Hybrid metal/polymer filaments for fused filament fabrication (FFF) to print metal parts. *Appl. Sci.* 11 (4), 1444.
- Trumbo P, Yates AA, Schlicker S, Poos M, 2001. Dietary reference intakes. *J. Am. Diet. Assoc.* 101 (3), 294–301. [PubMed: 11269606]
- Turner A, Filella M, 2021. Hazardous metal additives in plastics and their environmental impacts. *Environ. Int.* 156, 106622.
- US EPA, 1986. *Test Methods for Evaluating Solid Waste: Physical/Chemical Methods*, vol. 1. US Environmental Protection Agency, Washington, DC.
- US EPA, 2014. Method 6020B (SW-846): ICP-MS. United States Environmental Protection Agency, Washington, DC.
- US EPA, 2017. Method 1340: In Vitro Bioaccessibility Assay for Lead in Soil. United States Environmental Protection Agency, Washington, DC.
- Valino AD, Dizon JRC, Espera AH, Chen Q, Messman J, Advincula RC, 2019. Advances in 3D printing of thermoplastic polymer composites and nanocomposites. *Prog. Polym. Sci.* 98, 101162 10.1016/j.progpolymsci.2019.101162.
- Vance ME, Pegues V, Van Montfrans S, Leng W, Marr LC, 2017. Aerosol emissions from fuse-deposition modeling 3D printers in a chamber and in real indoor environments. *Environ. Sci. Technol.* 51 (17), 9516–9523. 10.1021/acs.est.7b01546. [PubMed: 28789516]
- Wang Y-L, Tsou M-C, Liao H-T, Hseu Z-Y, Dang W, Hsi H-C, Chien L-C, 2020. Influence of soil properties on the bioaccessibility of Cr and Ni in geologic serpentinite and anthropogenically contaminated non-serpentinite soils in Taiwan. *Sci. Total Environ.* 714, 136761 10.1016/j.scitotenv.2020.136761.
- Weidenhamer JD, Miller J, Guinn D, Pearson J, 2011. Bioavailability of cadmium in inexpensive jewelry. *Environ. Health Perspect.* 119 (7), 1029–1033. [PubMed: 21377949]
- Woods B, 2022. Beginner's FFF metal 3D printing guide. Retrieved from. <https://thevirtualfoundry.com/2022/06/20/fff-metal-3d-printing-guide/>.
- Yamamoto N, Takahashi Y, Yoshinaga J, Tanaka A, Shibata Y, 2006. Size distributions of soil particles adhered to children's hands. *Arch. Environ. Contam. Toxicol.* 51 (2), 157–163. 10.1007/s00244-005-7012-y. [PubMed: 16583253]
- Zhang H, Wang J, Zhou B, Zhou Y, Dai Z, Zhou Q, Luo Y, 2018. Enhanced adsorption of oxytetracycline to weathered microplastic polystyrene: kinetics, isotherms and influencing factors. *Environ. Pollut.* 243, 1550–1557. 10.1016/j.envpol.2018.09.122. [PubMed: 30296753]

HIGHLIGHTS

- Metal particles in thermoplastics are not chemically bound to the polymer and have potential for dermal adherence.
- Copper and bronze filaments release Cu particles that oxidize and dissolve in sweat.
- Simulated UV weathering increased rate of metal particle release.
- Wearing gloves and washing hands are suggested for use of metal-fill thermoplastics.

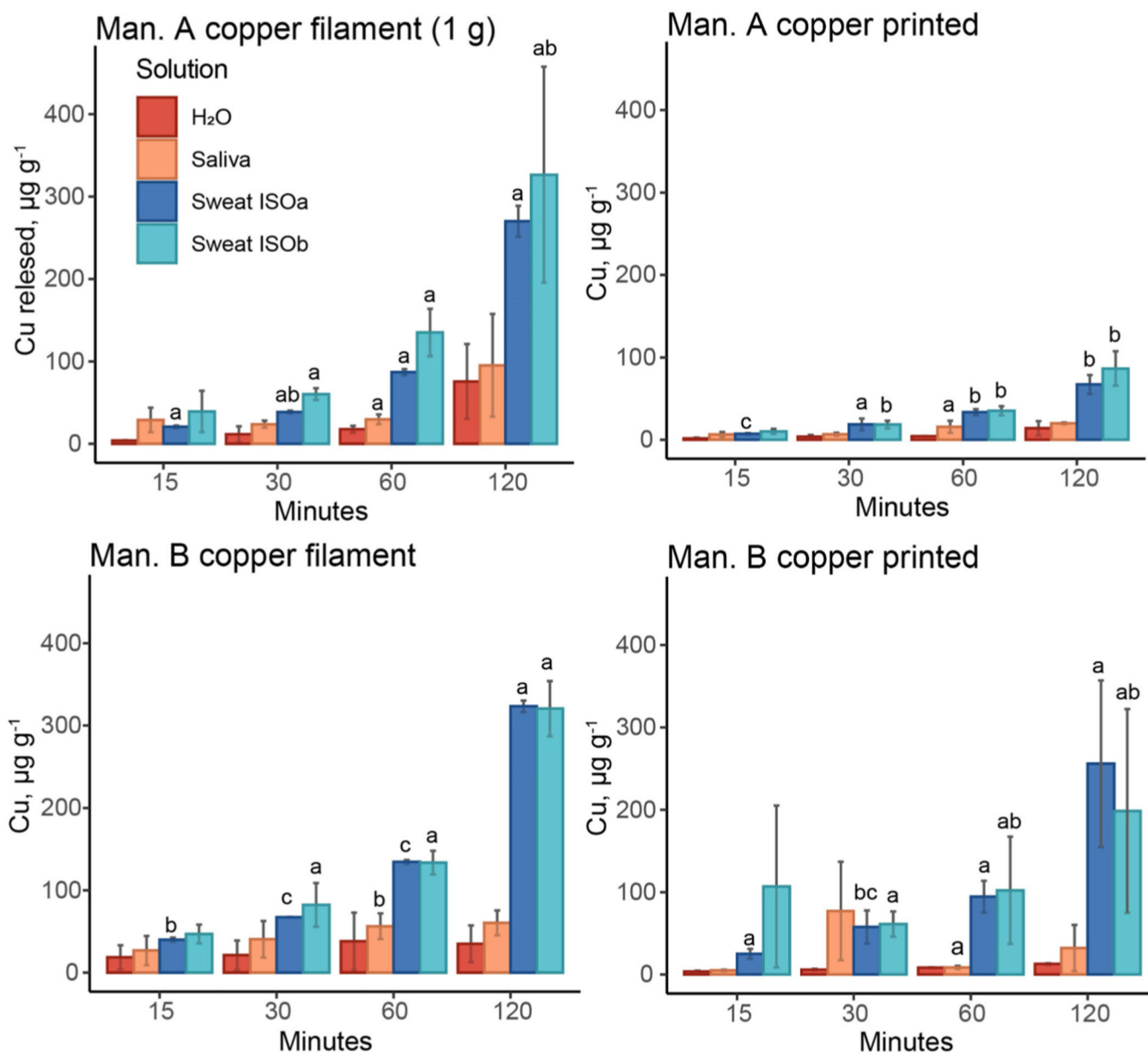


Fig. 1. Total Cu release (dissolved and particulate) in H₂O, synthetic saliva and synthetic sweats over two-hour period (n = 3). For each solution (H₂O, saliva, sweat ISOa, sweat ISOb), different lowercase letters indicate significant differences in Cu released from the 4 filament types (ANOVA and post-hoc Tukey's HSD test at p < 0.05) at each time point. For example, Man. B copper filament released significantly more Cu at 120 min than Man. A copper printed, but not significantly more than Man. A copper filament or Man. B copper printed.

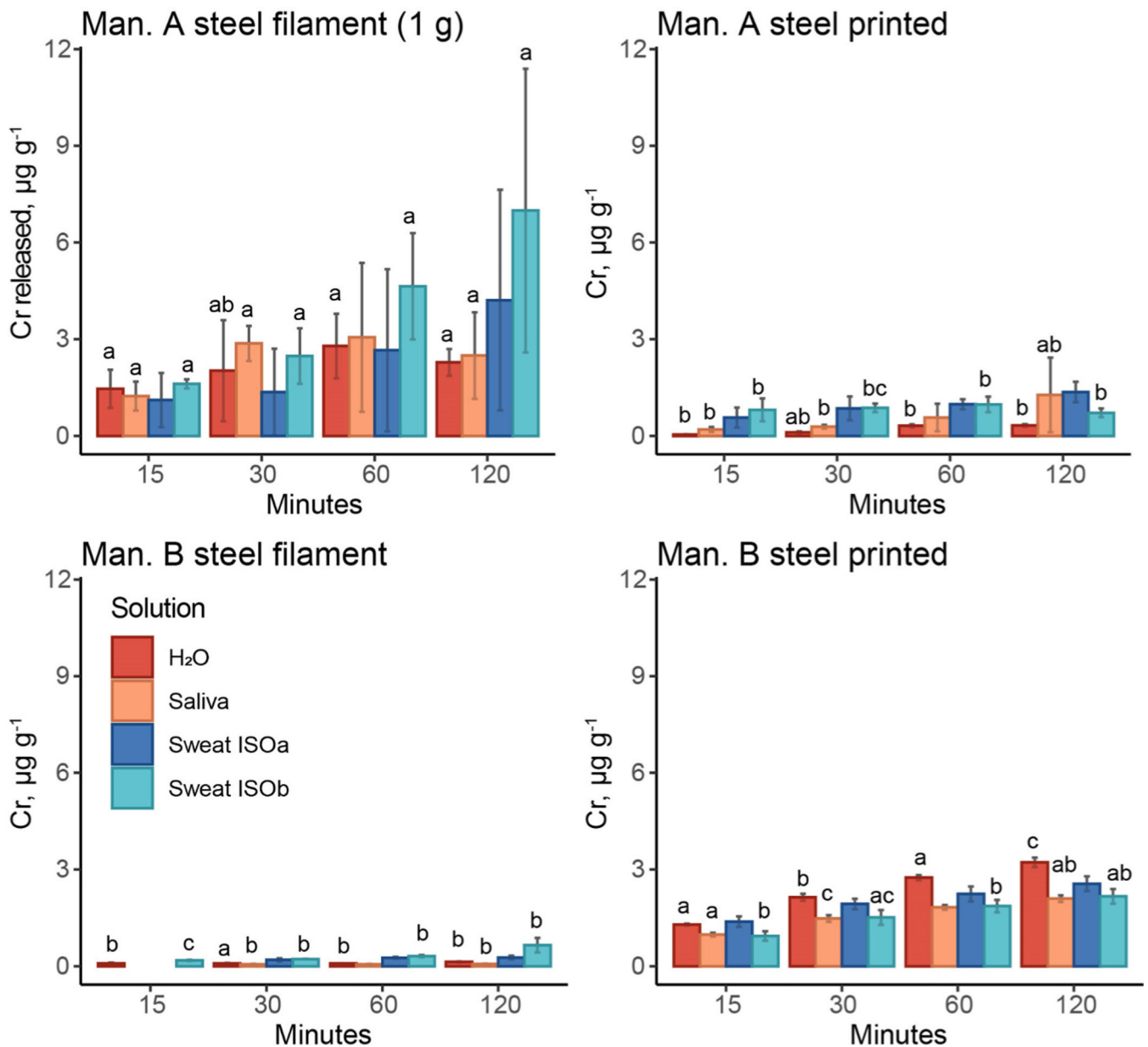


Fig. 2. Total Cr release (dissolved and particulate) in H₂O, synthetic saliva and synthetic sweats over two-hour period (n = 3). For each solution (H₂O, saliva, sweat ISOa, sweat ISOb), different lowercase letters indicate significant differences in Cr released from the 4 filament types (ANOVA and post-hoc Tukey's HSD test at p < 0.05) at each time point.

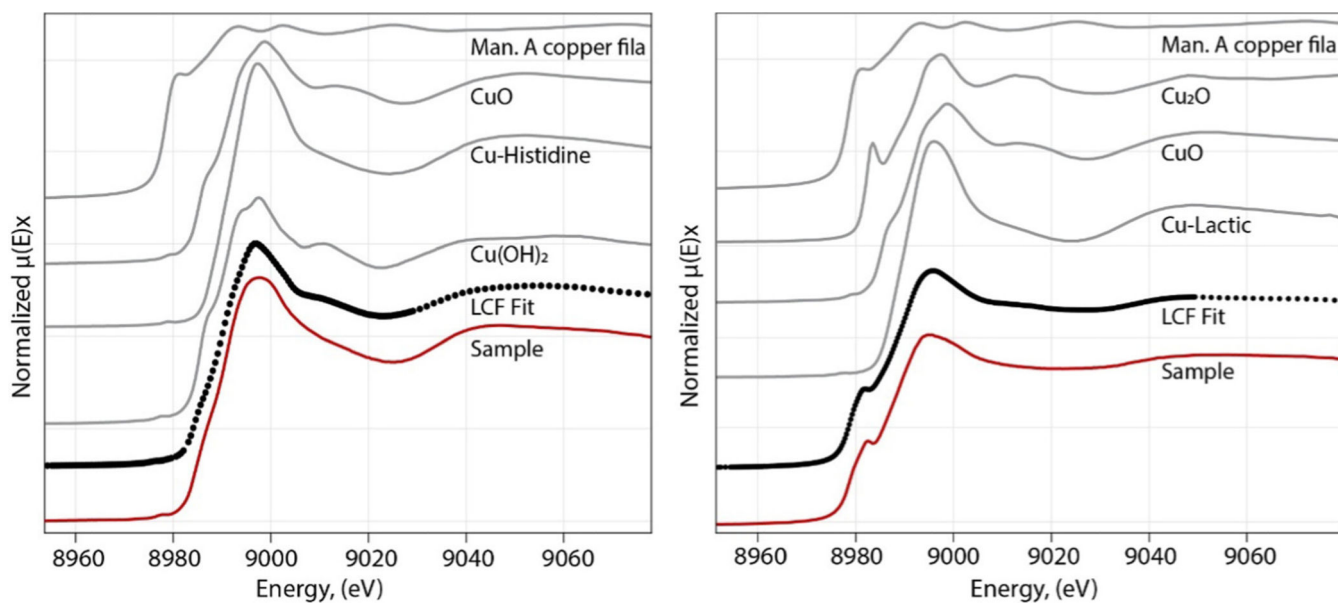


Fig. 3. Normalized Cu Ka XANES spectrum of Cu present on A) 10 kDa filter from Man. A copper filament in synthetic sweat ISOB after 24 h and B) 0.45 um filter from Man. A copper filament in IVBA extraction solution after 1 h along with reference compounds used for the LCF fit (fit range -20 to 30 eV above E_0). LCF fits presented as black circles.

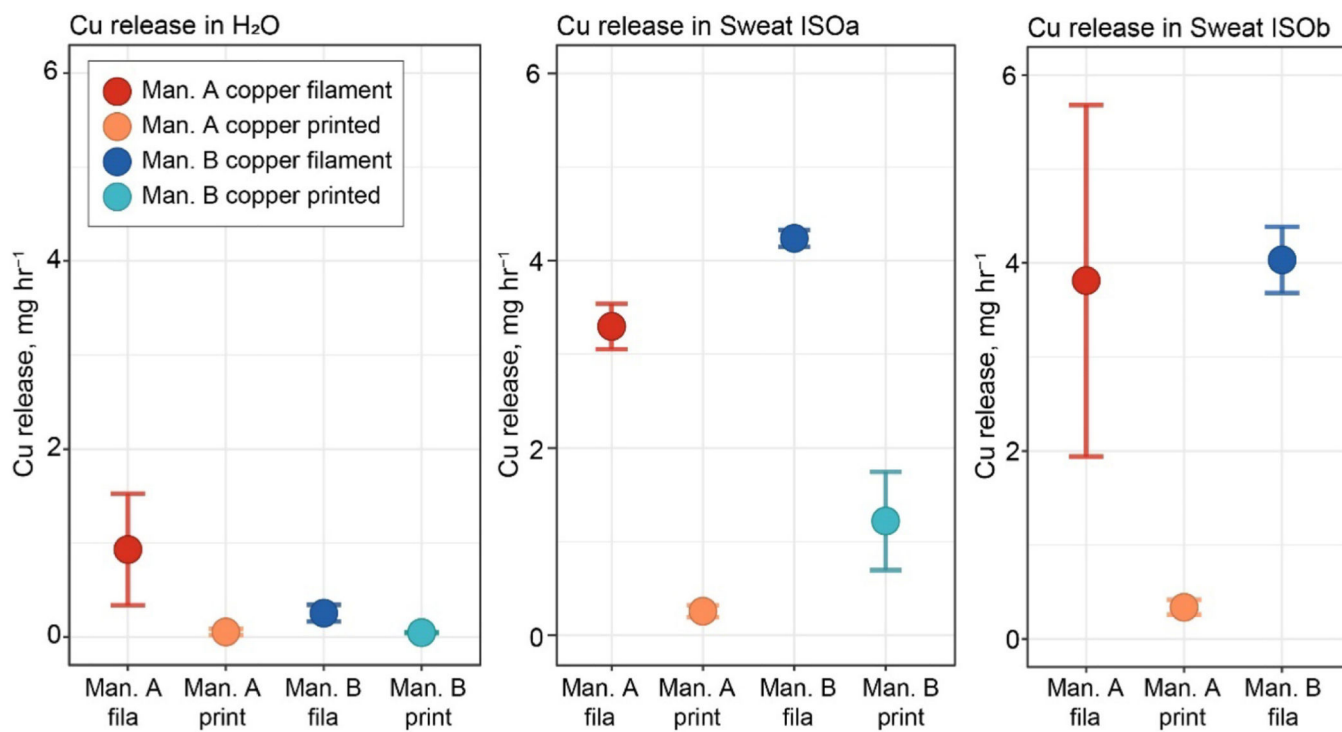


Fig. 4. Cu release rates, in mg h⁻¹, from a 5 cm³ cube in (1) H₂O, (2) synthetic sweat ISOa, and (3) synthetic sweat ISOb from copper filaments. Only model fits with p < 0.05 shown (n = 3 replicates). Full model fits are in SI Table A.8.

Table 1







Average concentration (\pm SD) of elements from filament digestions ($n = 3$). Total metal content in the filaments (bottom row) was determined by summing the total mass of the elements present.

Filament type	Man. A bronze	Man. B bronze	Man. A copper	Man. B copper	Man. A steel, 410L	Man. B steel, 316L
Major metals, mg g ⁻¹						
Cu	684 \pm 27	772 \pm 57	771 \pm 25	831 \pm 33		
Sn	86.5 \pm 3.7	94.2 \pm 6.7	0.32 \pm 0.01 *	0.09 \pm 0.01		
Cr					83.3 \pm 3.8	126 \pm 14 *
Mn					4.48 \pm 0.1 *	1.5 \pm 0.16
Fe					591 \pm 28	507 \pm 53
Mo						19.5 \pm 2.1 *
Ni						85.7 \pm 8.8 *
Trace metals, μ g g ⁻¹						
As	16.9 \pm 0.3 *	6.89 \pm 0.12	0.63 \pm 0.04	0.81 \pm 0.04	10.3 \pm 0.2	13.9 \pm 1.5
Cd		0.50 \pm 0.05 *		0.54 \pm 0.06		1.89 \pm 0.11 *
Co	4.64 \pm 0.21	5 \pm 0.05		1.71 \pm 0.11	284 \pm 2	523 \pm 36 *
Pb	28.2 \pm 0.1	155 \pm 3 *		42.5 \pm 0.9 *		
Sb	5.54 \pm 0.05	33.5 \pm 0.6 *		3.5 \pm 0.22		
Zn		1870 \pm 13 *		171 \pm 4		
Metal, %	77 \pm 3	87 \pm 6	77 \pm 3	83 \pm 3	68 \pm 3	74 \pm 6

(*) Asterisk indicates that there was significantly more of an element of metal present in the either the Man. A or the Man. B filament. Blanks indicate that an average was not detected, and italics indicate that it was not quantified. Elements not presented but included in the total metal calculation include silicon (Si), phosphorus (P), and potassium (K) (see SI Table A.3).

Table 2

Metallic particle diameter and specific surface area (SSA) in metal-fill filaments, including density distributions of data. CV = coefficient of variation. Mean and median SSA show combined surface area for 1 g of particles.

Filament	Mean, μm	Median, μm	CV, %	Particle size distribution	Density ^a g cm^{-3}	Mean SSA, $\text{m}^2 \text{g}^{-1}$	Median SSA, $\text{m}^2 \text{g}^{-1}$
Man. A copper	9.41	7.83	61		8.96	7.12 e^{-2}	8.59 e^{-2}
Man. B copper	12.4	7.72	101		8.96	5.40 e^{-2}	8.70 e^{-2}
Man. A bronze	19.8	16.5	62		8.73	3.47 e^{-2}	4.17 e^{-2}
Man. B bronze	12.3	9.30	76		8.73	5.59 e^{-2}	7.39 e^{-2}
Man. A steel, 410L	7.81	5.00	91		7.16	10.7 e^{-2}	16.8 e^{-2}
Man. B steel, 316L	24.0	23.1	39		8.00	3.25 e^{-2}	3.25 e^{-2}

^aDensity of metal alloys.

Table 3

Total metal release (coefficient of variation, CV % in parenthesis) from 1 g of printed or raw filament into different synthetic fluids following 2-hour extractions (n = 3).

Copper release, Cu, $\mu\text{g g}^{-1}$ (ppm)												
Fila. type	Man. A copper		Man. B copper		Man. A bronze		Man. B bronze		Man. A steel		Man. B steel	
	Filament	Printed	Filament	Printed	Filament	Printed	Filament	Printed	Filament	Printed	Filament	Printed
H ₂ O	75.8 (60)	14.0 (62)	35.2 (63)	12.8 (7.7)	<i>14.8*</i> (8.1)	8.38 (22)	34.5 (20)	20.5 (18)				
Saliva ¹	95.2 (65)	20.0 (5.4)	60.5 (25)	32.3 (87)	221 (78)	22.8 (49)	<i>78.1</i> (45)	35.7 (35)				
Sweat A ²	<i>270*</i> (7)	<i>67.2</i> (17)	323 (2.1)	256 (40)	131 (86)	62.0 (51)	237 (18)	366* (7.4)				
Sweat B ²	327 (40)	86.6 (24)	321 (10)	199 (62)	106 (95)	<i>17.6</i> (66)	125 (7.1)	225 (31)				
IVBA ³	406 (14)		681 (15)		584 (20)		1092 (2.7)					
SA, cm2 ^d	6.61	19.6	5.81	16.1	6.50	18.6	5.53	18.9				
Length, cm	11.8	12.5	10.4	102	11.6	118	9.9	120				
Chromium release, Cr, $\mu\text{g g}^{-1}$ (ppm)												
Fila. type	Man. A bronze		Man. B bronze		Man. A steel		Man. B steel		Man. A steel		Man. B steel	
	Filament	Printed	Filament	Printed	Filament	Printed	Filament	Printed	Filament	Printed	Filament	Printed
H ₂ O	<i>1.5*</i> (9.6)	<i>0.88</i> (28)	3.24 (42)	1.25 (33)	<i>2.28*</i> (18)	0.33 (12)	<i>0.14</i> (9.2)	<i>3.22*</i> (4.5)				
Saliva	25.7 (81)	2.66 (49)	8.34 (44)	3.66 (41)	2.49 (54)	1.27 (91)	<i>0.07</i> (9.9)	<i>2.10*</i> (5.0)				
Sweat A	13.9 (115)	6.13 (67)	15.6 (32)	13.8 (12)	4.21 (81)	1.36 (23)	0.27 (22)	<i>2.56*</i> (8.9)				
Sweat B	14.2 (97)	1.79 (72)	10.9 (11)	18.2 (44)	6.99 (63)	0.72 (19)	<i>0.65</i> (35)	<i>2.17*</i> (11)				
IVBA	72 (20)		121 (1.3)		82.2 (1.3)		0.65 (10)					
SA, cm2 ^d	See above				7.78	18.16	6.67	22.7				
Length, cm	See above				13.9	116	11.9	144				

* () indicates significant differences between filament and printed metal type ($p < 0.05$) of same manufacturer. Italics indicates values were not normally distributed based on Shapiro-Wilk test ($p = 0.05$). For chromium, note steel = stainless steel.

¹ Synthetic saliva, Standard EUR 19899 EN (2001).

² Synthetic sweat, Standard 105-E04:2013.

EPA Author Manuscript

EPA Author Manuscript

EPA Author Manuscript

³ TVBA, US EPA Method 1340 (2017).

^a Approximate surface area (S.A) of 1 g filament type.